






## Article

# Synthesis, Characterization, and Anticancer Activity of Phosphanegold(i) Complexes of 3-Thiosemicarbano-butan-2-one Oxime

Sani A. Zarewa <sup>1,†</sup>, Lama Binobaid <sup>2,†</sup>, Adam A. A. Sulaiman <sup>1,3,\*</sup>, Homood M. As Sobeai <sup>2</sup>, Moureq Alotaibi <sup>2</sup>, Ali Alhoshani <sup>2</sup> and Anvarhusein A. Isab <sup>1,4,\*</sup>

<sup>1</sup> Department of Chemistry, King Fahd University of Petroleum and Minerals, Dhahran 31261, Saudi Arabia; g202101570@kfupm.edu.sa

<sup>2</sup> Department of Pharmacology and Toxicology, College of Pharmacy, King Saud University, Riyadh 11451, Saudi Arabia; 442202864@student.ksu.edu.sa (L.B.); hassobeai@ksu.edu.sa (H.M.A.S.); mralotaibi@ksu.edu.sa (M.A.); ahoshani@ksu.edu.sa (A.A.)

<sup>3</sup> Core Research Facilities (CRF), King Fahd University of Petroleum and Minerals, Dhahran 31261, Saudi Arabia

<sup>4</sup> Interdisciplinary Research Center for Advanced Materials, King Fahd University of Petroleum and Minerals, Dhahran 31261, Saudi Arabia

\* Correspondence: adamahmed@kfupm.edu.sa (A.A.A.S.); aisab@kfupm.edu.sa (A.A.I.)

† These authors contributed equally to this work.

**Abstract:** Four novel phosphanegold(I) complexes of the type  $[\text{Au}(\text{PR}_3)(\text{DMT})].\text{PF}_6$  (**1–4**) were synthesized from 3-Thiosemicarbano-butan-2-one oxime ligand (TBO) and precursors  $[\text{Au}(\text{PR}_3)\text{Cl}]$ , (where R = methyl (**1**), ethyl (**2**), tert-butyl (**3**), and phenyl (**4**)). The resulting complexes were characterized by elemental analyses and melting point as well as various spectroscopic techniques, including FTIR and ( $^1\text{H}$ ,  $^{13}\text{C}$ , and  $^{31}\text{P}$ ) NMR spectroscopy. The spectroscopic data confirmed the coordination of TBO ligands to phosphanegold(I) moiety. The solution chemistry of complexes **1–4** indicated their stability in both dimethyl sulfoxide (DMSO) and a mixture of EtOH:H<sub>2</sub>O (1:1). In vitro cytotoxicity of the complexes was evaluated relative to cisplatin using an MTT assay against three different cancer cell lines: HCT116 (human colon cancer), MDA-MB-231 (human breast cancer), and B16 (murine skin cancer). Complexes **2**, **3**, and **4** exhibited significant cytotoxic effects against all tested cancer cell lines and showed significantly higher activity than cisplatin. To elucidate the mechanism underlying the cytotoxic effects of the phosphanegold(I) TBO complexes, various assays were employed, including mitochondrial membrane potential, ROS production, and gene expression analyses. The data obtained suggest that complex **2** exerts potent anticancer activity against breast cancer cells (MDA-MB-231) through the induction of oxidative stress, mitochondrial dysfunction, and apoptosis. Gene expression analyses showed an increase in the activity of the proapoptotic gene caspase-3 and a reduction in the activity of the antiapoptotic gene BCL-xL, which supported the findings that apoptosis had occurred.

**Keywords:** ligand; gold(I) complexes; anticancer evaluation; reactive oxygen species; action mechanism



**Citation:** Zarewa, S.A.; Binobaid, L.; Sulaiman, A.A.A.; Sobeai, H.M.A.; Alotaibi, M.; Alhoshani, A.; Isab, A.A. Synthesis, Characterization, and Anticancer Activity of Phosphanegold(i) Complexes of 3-Thiosemicarbano-butan-2-one Oxime. *Biomedicines* **2023**, *11*, 2512. <https://doi.org/10.3390/biomedicines11092512>

Academic Editor: Zhi Shi

Received: 22 July 2023

Revised: 23 August 2023

Accepted: 4 September 2023

Published: 12 September 2023



**Copyright:** © 2023 by the authors. Licensee MDPI, Basel, Switzerland. This article is an open access article distributed under the terms and conditions of the Creative Commons Attribution (CC BY) license (<https://creativecommons.org/licenses/by/4.0/>).

## 1. Introduction

Cancer is currently one of the most significant diseases that threaten the health of people worldwide. Despite the introduction of numerous new cancer diagnoses, the death rate in both industrialized and developing nations is rising [1,2]. Patients who undergo anticancer chemotherapy make up around half of those who are given platinum-based anticancer medications, like cisplatin and its variants [3,4]. Despite some incredible success, platinum-based chemotherapy for cancer is restricted due to its drug resistance and substantial side effects, which include ototoxicity, neurotoxicity, and nephrotoxicity [5–7]. These adverse effects result from the innate incapacity of these cytotoxic medicines to

distinguish between cancer cells and normal cells. This has motivated researchers to synthesize novel metal-based antitumor agents with various modes of action and coordination characteristics [8].

It has been established that thiosemicarbazones are a significant class of possible binding sites for multidentate compounds for a variety of metal ions [9–11]. A five-membered chelate ring or a four-membered ring with high strain is often formed by either the azomethine N or the sulfur group or the hydrazine N atom [11–13]. S-monodentate is one of the additional coordination modes seen in thiosemicarbazone complexes (Figure 1) [13]. Thiosemicarbazones are adaptable pharmacophores, due to their ability to form stable compounds with transition metal ions [14,15]. It is well known that thiosemicarbazones have antioxidant, antiviral, and DNA-binding properties [16–19]. The commercialized methisazone, (trade name Marboran<sup>®</sup>: Burroughs Wellcome & Co., London, England), used to treat smallpox and the anticancer drug 3-aminopyridine-2-carboxaldehyde thiosemicarbazone (trade name Triapine<sup>®</sup>, Vion Pharmaceuticals, Inc., New Haven, CT, USA) have progressed to phase II clinical testing for use against a variety of cancers. The anticancer activity of thiosemicarbazone metal complexes is dependent on the type of tumor cells [19]. It is interesting to note that thiosemicarbazones have been shown to be more active or to have much fewer adverse effects when they are coordinated with metal ions [20]. Thiosemicarbazones and their complexes have cytotoxic activity owing to their capacity to inhibit enzymes, like ribonucleotide reductase, topoisomerase II, and multidrug-resistant protein (MDR1), by interfering with mitochondrial function and releasing reactive oxygen species (ROS) [21–25].

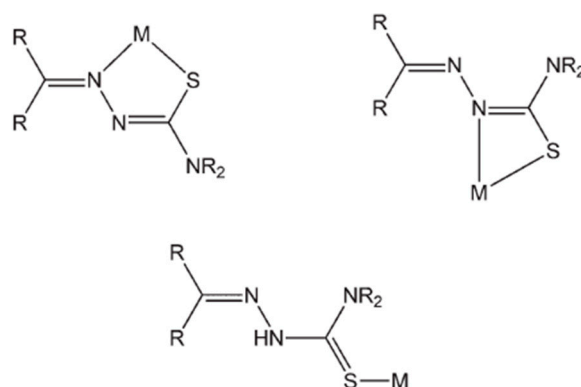
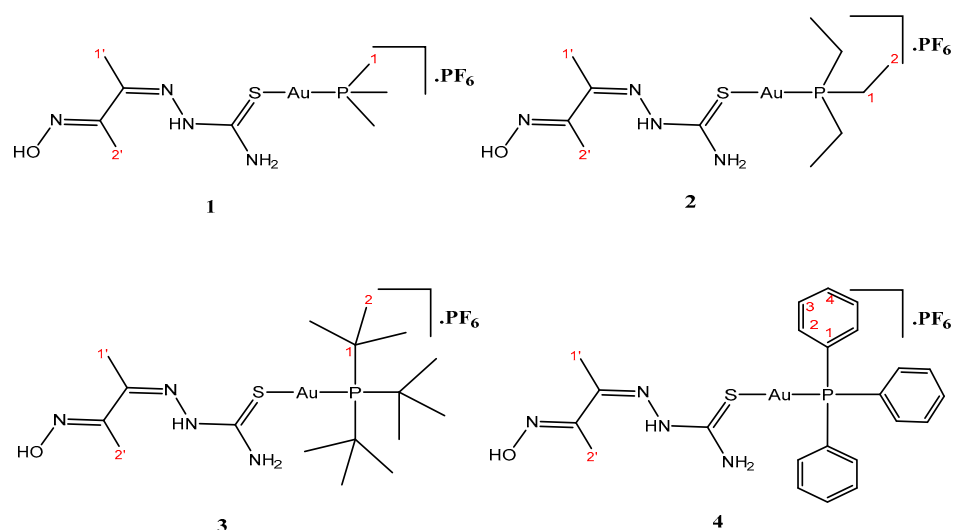


**Figure 1.** Different coordination mechanisms in thiosemicarbazone ligand complexes with metals.

The investigation of gold complexes with various functional ligands that exhibit intriguing physical, chemical, biological, and pharmacological properties has garnered significant interest in recent years [26–29]. Specifically, gold(I) complexes that contain phosphane ligands have displayed anticancer properties, making them a compelling area of study [29–33]. The literature sources have shown that the incorporation of phosphine ligands into gold(I) complexes can enhance their potency and/or generate selectivity for a range of biological targets. The gold complexes that included phosphine derivatives exhibited better biological responses and higher selectivity indices compared to their nonphosphine counterparts. In this regard, Auranofin has exhibited notable cytotoxic activity in various in vitro and in vivo tumor models, including those that are resistant to cisplatin [34–36]. Gold(I)–phosphane complexes have been shown to accumulate selectively in mitochondria, suggesting that this organelle may be their primary site of biological activity. The complexes' cytotoxic effects appear to be associated with their capacity to bind and inhibit thioredoxin reductase (TrxR), a mitochondrial enzyme, or other thiol-rich proteins and enzymes, leading to their anticancer properties and ability to induce cell apoptosis via reactive oxygen species (ROS) [33,37]. The complexes also effectively inhibit TrxR compared to the free ligands [38].

Tavares and colleagues investigated the cytotoxic properties of gold(I) complexes with aryl-thiosemicarbazones on B16-F10 and CT26.WT tumor cells, as well as BHK-21 nontumor cells. Most of the tested complexes demonstrated moderate cytotoxic activity, with some greater cytotoxicity than cisplatin [38]. González-Barcia and colleagues examined the cytotoxicity of phosphine–thiosemicarbazone gold(I) complexes against several human tumor cell lines, including ovarian adenocarcinoma (MCF-7), cervical epithelial carcinoma (HeLa 229), non-small cell lung cancer (NCI-H460), and normal human lung fibroblast (MRC5) in vitro. The complexes also demonstrated potent inhibition of the activity of thioredoxin reductase and an enzyme crucial for cellular redox signaling [39].

Due to the favorable properties of gold(I) complexes as a viable alternative to Pt agents, coupled with the scarcity of studies regarding gold(I)phosphine complexes with thiosemicarbazone ligands [38,39], and in continuation of our interest in the development of next-generation anticancer gold(I) metallodrugs, herein we report the synthesis and characterization of thiosemicarbazone ligand derived from diacetylmonoxime, and complexation with phosphane-gold(I) for the first time in order to develop unique next-generation anti-tumor metal agents, perhaps maybe with fewer side effects than anticancer medications currently available in the markets. The described complexes 1–4 (shown in Scheme 1) are characterized by the spectroscopic methods UV-Vis, FTIR, NMR studies, and elemental analyses. In vitro tests on their cytotoxicity against HCT116 (human colon cancer), MDA-MB-231 (human breast cancer), and B16 (murine skin cancer) were evaluated.



**Scheme 1.** Structure of the gold(I) 1–4 complexes with resonance assignments.

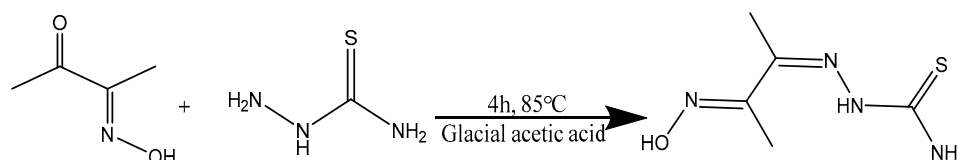
## 2. Materials and Methods

### 2.1. General

Diacetylmonoxime and thiosemicarbazide were purchased from Sigma-Aldrich Co., St. Louis, MO, USA. The compounds Bromo(tri-methylphosphine), chloro(tri-ethylphosphine), chloro(tri-tert-butylphosphine), and chloro(tri-phenylphosphine) were purchased from Strem Chemicals, Inc., Newburyport, MA, USA. Dichloromethane and ethanol were provided by Merck KGaA, Darmstadt, Germany and were used directly without further purification. The melting points were measured using a Büchi Melting Point M-560 device from Büchi, Switzerland. Elemental analyses were performed on the PerkinElmer Series II (CHNS/O) Analyzer 2400 series, Shelton, CT, USA.  $^1\text{H}$  and  $^{13}\text{C}$  NMR spectra were acquired on a Bruker 400 spectrophotometer, MA, USA., while  $^{31}\text{P}$  NMR spectra were acquired on JEOL 600, JASTEC Superconductor, Hyogo, Japan. On a NICOLET 6700 FTIR, Thermo Electron Corporation, Madison, WI, USA, employing potassium bromide (KBr) pellets over range of  $400\text{--}400\text{ cm}^{-1}$ . The solid-state FTIR spectra of free ligands and their phosphane-gold(I) complexes were collected.

## 2.2. Synthesis of Ligand (TBO)

The ligand (**TBO**) was prepared by adding an ethanolic solution (20 mL) of diacetylmonoxime (101.105 mg, 1 mmol) to a well-stirred warm ethanolic solution (20 mL) of thiosemicarbazide (91.14 mg, 1 mmol) with a few drops of glacial acetic acid. The solution was refluxed for four hours at 80 °C. The reaction mixture was then concentrated to half and cooled down to room temperature to afford the crystalline product, which was re-crystallized and collected by filtration and dried in a desiccator over CaCl<sub>2</sub> (Scheme 2).



**Scheme 2.** Synthesis of ligand TBO.

**Ligand (TBO):** Yield = 0.176 g (92%). M.P: 202.5 °C. Anal. Calcd. for C<sub>5</sub>H<sub>10</sub>N<sub>4</sub>SO: MW g/mol C, 34.47; H, 5.79; N, 32.16; S, 18.40. Found: C, 34.75; H, 5.39; N, 31.50; S, 18.22. IR (KBr, cm<sup>-1</sup>): 3415 ν(OH), 3264, 3238 ν(NH<sub>2</sub>), 3156 ν(N-H), 1598 ν(C=N-OH), 1494 ν(C=N), 1374, 1286, 845 ν(-N-C=S). <sup>1</sup>H NMR (400 MHz, DMSO) δ 11.57 (OH, s, 1H), 10.19 (NH, s, 1H), 8.34 (NH<sub>2</sub>, s, 1H), 7.75 (NH<sub>2</sub>, s, 1H), 2.08 (H1', s, 3H), 1.99 (H2', s, 3H). <sup>13</sup>C NMR (101 MHz, DMSO) δ 179.00 (C=S), 154.72 (C=N-OH), 147.46 (C=N-N), 11.76 (C1'), 9.38 (C2').

## 2.3. Synthesis of [Au(PR<sub>3</sub>)(TBO)]PF<sub>6</sub> Complexes (1–4)

Complexes **1–4** were prepared by combining AgPF<sub>6</sub> (0.126 g, 0.5 mmol) dissolved in 10 mL ethanol with Me<sub>3</sub>PAuBr(**1**) (0.176 g, 0.5 mmol), Et<sub>3</sub>PAuCl(**2**) (0.175 g, 0.5 mmol), t-But<sub>3</sub>PAuCl(**3**) (0.217 g, 0.5 mmol), and Ph<sub>3</sub>PAuCl(**4**) (0.247 g, 0.5 mmol) in 10 mL dichloromethane. The mixture was stirred at room temperature for 15 min and filtered off to remove AgBr and AgCl as yellow and white precipitates, respectively. The filtrate of each complex was then added to respective ligand **TBO** (0.087 g, 0.5 mmol) dissolved in 10 mL ethanol. After two hours of stirring, the solution was filtered. The pale-yellow solutions were kept at room temperature. After some days, white to yellow crystals were obtained. The obtained crystals were recrystallized from a mixture of acetone/acetonitrile (1:1).

**[(Me)<sub>3</sub>PAu(TBO)].PF<sub>6</sub> 1:** Yield: 0.14 g (47%) M.P: 141–145 °C. Anal. Calcd. for C<sub>8</sub>H<sub>19</sub>AuF<sub>6</sub>N<sub>4</sub>P<sub>2</sub>SO: MW = 592.23 g/mol: C, 16.22; H, 3.23; N, 9.46; S, 5.41. Found: C, 15.79; H, 2.97; N, 9.02; S, 5.14. IR (KBr, cm<sup>-1</sup>): 3427 ν(OH), 3248, 3222 ν(NH<sub>2</sub>), 3165 ν(N-H), 1605 ν(C=N-OH), 1507 ν(C=N), 1365, 1294, 845 ν(-N-C=S). <sup>1</sup>H NMR (400 MHz, DMSO) δ 11.84 (OH, s, 1H), 10.94 (NH, s, 1H), 9.09 (NH<sub>2</sub>, s, 1H), 8.40 (NH<sub>2</sub>, s, 1H), 2.14 (H1', s, 3H), 2.02 (H2', s, 3H), 1.63 (H1, d, J = 11.9 Hz, 6H). <sup>13</sup>C NMR (101 MHz, DMSO) δ 174.00 (C=S), 154.59 (C=N-OH), 152.77 (C=N-N), 14.71, 14.33 (C1), 12.38 (C1'), 9.52 (C2'). J-value <sup>13</sup>C NMR (101 MHz, DMSO) δ 14.52 (C1, d, J = 38.5 Hz). <sup>31</sup>P NMR (600 MHz, DMSO) δ 0.089, -143.591 (PF<sub>6</sub>).

**[(Et)<sub>3</sub>PAu(TBO)].PF<sub>6</sub> 2:** Yield = 0.19 g (59%). M.P: 157–160 °C. Calc. for C<sub>11</sub>H<sub>25</sub>AuF<sub>6</sub>N<sub>4</sub>P<sub>2</sub>S: MW = 634.31 g/mol: C, 20.83; H, 3.97; N, 8.83; S, 5.06. Found: C, 20.77; H, 3.85; N, 9.06; S, 5.13. IR (KBr, cm<sup>-1</sup>): 3429 ν(OH), 3247, 3220 ν(NH<sub>2</sub>), 3165 ν(N-H), 1607 ν(C=N-OH), 1508 ν(C=N), 1367, 1297, 842 ν(-N-C=S). <sup>1</sup>H NMR (400 MHz, DMSO) δ 11.76 (OH, s, 1H), 10.80 (NH, s, 1H), 8.96 (NH<sub>2</sub>, s, 1H), 8.28 (NH<sub>2</sub>, s, 1H), 2.13 (H1', s, 4H), 2.02 (H2', s, 3H), 1.94 (H1, d, J = 7.7 Hz, 7H), 1.12 (H2, d, J = 19.1 Hz, 10H). <sup>13</sup>C NMR (101 MHz, DMSO) δ 174.04 (C=S), 154.50 (C=N-OH), 152.45 (C=N-N), 16.97, 16.61 (C1), 12.28 (C1'), 9.42 (C2'), 8.97 (C2). J-value: <sup>13</sup>C NMR (101 MHz, DMSO) δ 16.79 (C1, d, J = 35.3 Hz), 9.20 (d, J = 45.4 Hz). <sup>31</sup>P NMR (600 MHz, DMSO) δ 36.899, -143.591 (PF<sub>6</sub>).

**[(t-But)<sub>3</sub>PAu(TBO)].PF<sub>6</sub> 3:** Yield = 0.25 g (69%). M.P: 168.5–169.3 °C. Calc. for C<sub>17</sub>H<sub>37</sub>AuF<sub>6</sub>N<sub>4</sub>P<sub>2</sub>S: MW = 718.47 g/mol: C, 30.47; H, 2.94; N, 4.30; S, 4.93. Found: C, 31.46; H, 2.21; N, 3.72; S, 4.55. IR (KBr, cm<sup>-1</sup>): 3429 ν(OH), 3248, 3220 ν(NH<sub>2</sub>), 3165 ν(N-H), 1607 ν(C=N-OH), 1508 ν(C=N), 1370, 1297, 838 ν(-N-C=S). <sup>1</sup>H NMR (400 MHz, DMSO) δ

11.79 (OH, s, 1H), 10.95 (NH, s, 1H), 9.11 (NH<sub>2</sub>, s, 1H), 8.42 (NH<sub>2</sub>, s, 1H), 2.14 (H1', s, 3H), 2.02 (H2', s, 3H), 1.48 (H2, d, *J* = 13.9 Hz, 27H). <sup>13</sup>C NMR (101 MHz, DMSO) δ 174.02 (C=S), 154.50 (C=N-OH), 152.08 (C=N-N), 31.80 (C2), 29.55 (C1), 12.26 (C1'), 9.41 (C2'). <sup>31</sup>P NMR (600 MHz, DMSO) δ 97.021, -143.591 (PF<sub>6</sub>).

**[(Ph)<sub>3</sub>PAu(TBO)].PF<sub>6</sub> 4:** Yield = 0.22 g (56%). M.P: 181–183. Calc. for C<sub>17</sub>H<sub>37</sub>AuF<sub>6</sub>N<sub>4</sub>P<sub>2</sub>S: MW = 778.44 g/mol: C, 30.47; H, 2.94; N, 4.30; S, 4.93. Found: C, 31.46; H, 2.21; N, 3.72; S, 4.55. IR (KBr, cm<sup>-1</sup>): 3428 ν(OH), 3246, 3221 ν(NH<sub>2</sub>), 3158 ν(N-H), 1605 ν(C=N-OH), 1507 ν(C=N), 1367, 1295, 841 ν(-N-C=S). <sup>1</sup>H NMR (400 MHz, DMSO) δ 11.67 (OH, s, 1H), 10.55 (NH, s, 1H), 8.72 (NH<sub>2</sub>, s, 1H), 8.06 (NH<sub>2</sub>, s, 1H), 7.74–7.19 (H2, H3, H4, m, 15H), 2.10 (H1', s, 3H), 2.01 (H2', s, 3H). <sup>13</sup>C NMR (101 MHz, DMSO) δ 176.59 (C=S), 154.60 (C=N-OH), 149.73 (C=N-N), 133.99, 133.86, 132.39, 129.77, 129.66 (C1–C4), 12.00, 9.38. <sup>31</sup>P NMR (600 MHz, DMSO) δ 36.792, -143.591 (PF<sub>6</sub>).

#### 2.4. Cell Culture

HCT116, MDA-MB-231, and B16 cells were acquired from American Type Culture Collection (ATCC, Manassas, VA, USA). They were grown in DMEM, 10% fetal bovine serum (FBS), and 1% Penicillin/Streptomycin. All cells were incubated in a humidified chamber at 37 °C with 5% CO<sub>2</sub>.

#### 2.5. Cell Viability Assay

To evaluate the cell viability effect of novel complexes (**TBO**, **1**, **2**, **3**, and **4**) on cancer cell lines HCT116 (human colon cancer), MDA-MB-231 (human breast cancer), and B16 (murine skin cancer), 1 × 10<sup>4</sup> cells were seeded with 200 μL culture media in each well of a 96-well plate and incubated for 24 h. Next, the media were removed, and cells were exposed to different concentrations (1, 3, 10, 30, and 100 μM) of each complex, cisplatin (a positive control), and untreated cells as negative control. Then, the plates containing the drugs were incubated for 24 h. Later, 15 μL serum-free medium containing 5 mg/mL MTT dye (3-(4,5-dimethylthiazol-2-yl)-2,5-diphenyltetrazolium bromide) was added to each well and incubated for 2 h in the CO<sub>2</sub> incubator at 37 °C. The formazan crystals were dissolved in 200 μL of isopropyl alcohol after removing MTT dye and drug-containing media. The absorbance indicating cell viability was measured using a microplate reader at 570 nm wavelength. The following formula was used to calculate the percentage of cell viability: Cell viability % = 100 × (AbsorbanceCompound)/(AbsorbanceControl). The IC<sub>50</sub> value of the novel groups and cisplatin were calculated in μM using Excel and Graph-Pad Prism version 9.3 (Graph-Pad software, San Diego, CA, USA).

#### 2.6. Mitochondrial Membrane Potential (ΔΨ<sub>m</sub>) Assay

A total of 1 × 10<sup>4</sup> cells of MDA-MB-231 were cultured in 200 μL culture medium per well in a 96-well plate. Concentrations of 0.3, 1, 3, and 5 μM of the novel complex **2** and control wells were used in this experiment to determine the shift in mitochondrial depolarization. The 96-well plate was incubated for 24 h. Afterward, with the use of the JC-1 apoptosis detection kit, cells were incubated for 30 min. ΔΨ<sub>m</sub> alterations were measured by red/green fluorescence emission with excitation/emission 560/595 nm and 485/535 nm, respectively. Visualization of fluorescence was by the Synergy H1 fluorescent microplate reader. Quantification of the ratio of J-aggregate to JC-1 monomer intensity was calculated by counting for loss in ΔΨ<sub>m</sub> as a decrease in the of aggregate/monomer ratio, while an increase in ΔΨ<sub>m</sub> implied an increase in the ratio.

#### 2.7. ROS Assay

A total of cells 1 × 10<sup>4</sup> MDA-MB-231 were cultured in 200 μL culture medium per well in 96-well plates. Then, they were treated at concentrations of 0.3, 1, and 3 μM of complex **2**, and control wells were replaced with fresh media. The plates were incubated for 1–2 h, and 50 μL of 25 μM concentration of the fluorescent dye 2',7'-dichlorodihydrofluorescein diacetate (H<sub>2</sub>DCFDA) was added to each well and incubated for 30 min at 37 °C in 5% CO<sub>2</sub>

humidity. A total of 500  $\mu\text{M}$  of  $\text{H}_2\text{O}_2$  was used as positive control. The plates were read with Synergy H1 fluorescent microplate reader (ThermoFisher, Waltham, MA, USA) with excitation of 485 nm/emission 535 nm.

### 2.8. Quantitative Reverse Transcription-Polymerase Chain Reaction (qRT-PCR)

The extraction of total RNA was carried out with RNAbler Kit (Haven Scientific, Thuwal, Saudi Arabia) as indicated by the protocol. RNA concentration and purity, at a 260/280 ratio of  $\sim 2.0$ , were measured by nanodrop (NanoDrop Lite Plus, Thermo Scientific, USA). Later, the extracted RNA was reverse-transcribed into cDNA using the High-Capacity cDNA reverse transcription kit (Applied Biosystems®; Thermo Fisher Scientific, Inc. USA) in a thermocycler. The second step of qRT-PCR was by using a QuantStudio 6 Flex system (Thermo Fisher Scientific, Inc., Franklin, MA, USA) for qPCR reactions with the use of EverGreen 2 $\times$  PCR Master Mix (Haven Scientific, Thuwal, Saudi Arabia). GAPDH was served as the housekeeping gene for the qPCR step. The thermocycling conditions were as follows: 95 °C for 10 s; 60 °C for 20 s; and 72 °C for 10 s and a total of 40 cycles. Calculation of the relative gene expression was conducted using the comparative cycle threshold (CT) ( $2^{-\Delta\Delta\text{CT}}$ ) method. The specific forward and reverse primer sequences (synthesized and purchased from Invitrogen) were as follows:

GAPDH: forward 5'-AGC CAC ATC GCT CAG ACA C-3' and reverse 5'-GCC CAA TAC GAC CAA ATC C-3'.

BCL-xL: forward 5'-CTG AAT CGG AGA TGG AGA CC-3' and reverse 5'-TGG GAT GTC AGG TCA CTG AA-30'.

Caspase-3: forward 5'-GAG TGC TCG CAG CTC ATA CCT-3' and reverse 5'-CCT CAC GGC CTG GGA TTT-3'.

### 2.9. Solution Chemistry of Complexes (1–4)

To investigate the stability of complexes 1–4 recorded on GENESYS 10S UV-Vis spectrophotometer, Thermo Scientific, Franklin, MA, USA. The complexes were dissolved separately in DMSO and a solution containing EtOH:H<sub>2</sub>O (1:1) and subsequently analyzed for stability during period of 0 h, 12 h, 24 h, and 48 h.

## 3. Results

### 3.1. Preparation and FT-IR Characterization

The synthesis of the complexes (1–4) involved a two-step chemical process. In the initial stage, the starting complexes chloro(tri-methylphosphine)gold(I), chloro(tri-ethylphosphine)gold(I), chloro(tri-tert-butylphosphine)gold(I), and chloro(tri-phenylphosphine)gold(I) were mixed with silver hexafluorophosphate in a 1:1 molar ratio. Then, an equimolar amount of TBO ligand was added after filtering off the AgCl precipitate. The resulting  $[\text{Au}(\text{PR}_3)(\text{TBO})]\text{PF}_6$  complexes (1–4) were isolated as dry crystalline solids. Based on elemental analyses results, the stoichiometry of the complexes was established. The results of the elemental analyses for the free ligand (TBO) and the gold(I) complexes 1–4 are listed in Table S1. Complexes possess stability against air and heat, exhibiting a melting point in the range of 140–180 °C.

The IR characteristic wavenumber peaks for free ligand (TBO) and its complexes (1–4) are summarized in Table S2, while the FT-IR spectra of the compounds are provided in Supplementary Figures S1–S5. The bonding between the ligand and the metal ion is determined by comparing the IR spectra of the free ligand and its complexes. In the IR spectrum of the ligand (TBO), a distinct peak at  $3415\text{ cm}^{-1}$  was observed, indicating  $\nu(\text{OH})$  stretching vibrations. The bands of  $\nu(\text{NH}_2)$  and  $\nu(\text{NH})$  appeared at  $3264/3238$  and  $3156\text{ cm}^{-1}$ , respectively [40]. Additionally, two other bands detected at  $1598$  and  $1494\text{ cm}^{-1}$  were attributed to  $\nu(\text{C}=\text{N}-\text{OH})$  and  $\nu(\text{C}=\text{N})$ , respectively [41,42]. The results confirm the synthesis of the TBO ligand. Comparing the IR data of the complexes (1–4) to that of the free ligand, the frequency of the  $\nu(\text{NH}_2)$  group in the complexes shifted toward lower frequencies by 16, 17, or  $18\text{ cm}^{-1}$  due to the interaction between the NH and

NH<sub>2</sub> groups, leading to two distinct forms of intra- and intermolecular hydrogen bonding involving imine groups. Similar structures of complexes have been documented in the literature [40,43]. It was observed that the position of the thioamide  $\nu(\text{HN}-\text{C}=\text{S})$  bands of thiosemicarbazone appeared at 1374, 1286, and 845 cm<sup>-1</sup>, which are the result of mixed vibrations that combine C–N stretching, C=S stretching, and NH bending [44,45]. The frequencies shifted 4–10 cm<sup>-1</sup> toward lower wave numbers in the complexes (as shown in Table S2). This shift indicates that the sulfur of thione is involved in the coordination with the metal ion.

### 3.2. NMR Characterization

The NMR spectra of the free ligand (TBO) and its complexes were carried out in a DMSO-d<sub>6</sub> solution. The <sup>1</sup>H NMR chemical shifts of both the free ligand and its corresponding complexes (1–4) are given in Table 1. The <sup>1</sup>H NMR data of free ligand (TBO) revealed signals at 2.08 and 1.99 ppm (methyl protons H1', H2'); 7.75 and 8.34 ppm (NH<sub>2</sub>); 10.19 ppm (NH); and 11.57 ppm (OH). The two distinct singlet signals for –NH<sub>2</sub> proton indicate that the partial double-bond nature prevents the C–N bond from revolving freely, which is shown in (Figure S6). In the <sup>1</sup>H NMR chemical shifts of gold(I) complexes (1–4), the signal of the OH group appeared at 11.67–11.84 ppm appeared relatively downfield with a little shift in the range of 0.27–0.1 ppm with respect to free ligand (TBO), indicating the protonated nature of the C=N–OH group. A little downfield shift in the (NH and NH<sub>2</sub>) peaks of the complexes at 10.55–10.94 ppm for (NH) and at 8.72–9.1/8.06–8.42 ppm for (NH<sub>2</sub>) vs. free ligand that observed at 10.19 ppm for (NH) and 7.75/8.34 ppm for (NH<sub>2</sub>). The observed downfield shifts indicating the coordination of the gold(I) center to the sulfur of the thione group. The little shifts in protons of the NH<sub>2</sub> group is attributed to a potential hydrogen bonding between the amino group and solvent (NH<sub>2</sub> . . . DMSO) [38,45,46].

**Table 1.** <sup>1</sup>H NMR chemical shifts ( $\delta$ ) of free ligand and its complexes (1–4) carried out in (DMSO-d<sub>6</sub>) solution.

Compounds	OH	NH	NH <sub>2</sub>	H1'	H2'	H1	H2	H3	H4
TBO	11.57	10.19	8.34, 7.75	2.08	1.99	-	-	-	-
1	11.84	10.94	9.09, 8.40	2.14	2.02	1.63	-	-	-
2	11.76	10.80	8.96, 8.28	2.13	2.02	1.94	1.12	-	-
3	11.79	10.95	9.11, 8.42	2.14	2.02	-	1.48	-	-
4	11.67	10.55	8.72, 8.06	2.10	2.01	-	7.56	7.59	7.61

<sup>13</sup>C NMR chemical shift data are presented in Table 2. The <sup>13</sup>C NMR data of ligand TBO showed peaks at 9.38 (C1'), 11.76 (C2'), 147.46 (C=N–N), 154.72 (C=N–OH), and 179.00 ppm (C=S), which are in accordance with the literature [45,47,48]. In the gold(I) complexes (1–4), the C=N–N signals appeared in the range of 149.73–152.77 ppm compared to the free ligand at 147.46 ppm. The up-shift of C=S in the complexes proved the coordination of the thione sulfur to the gold center, which was identified at 179 ppm in the free ligand (TBO). The <sup>31</sup>P NMR data of complexes (1–4) showed single resonance at 0.089 ppm (1), 36.98 ppm (2), 97.0 ppm (3), and 36.79 ppm (4) with respect to the precursors appeared at –9.66 ppm (1), 32.0 ppm (2), 91.15 ppm (3), and 33.8 ppm (4). The downfield shift in the range of (2.974–9.751) ppm compared to the phosphane of the precursors is shown in Table S3. <sup>31</sup>P NMR data confirmed the synthesized complexes and are in agreement with (<sup>1</sup>H, <sup>13</sup>C) NMR and IR data. <sup>1</sup>H, <sup>13</sup>C, and <sup>31</sup>P NMR spectra are given in Figures S6–S19.

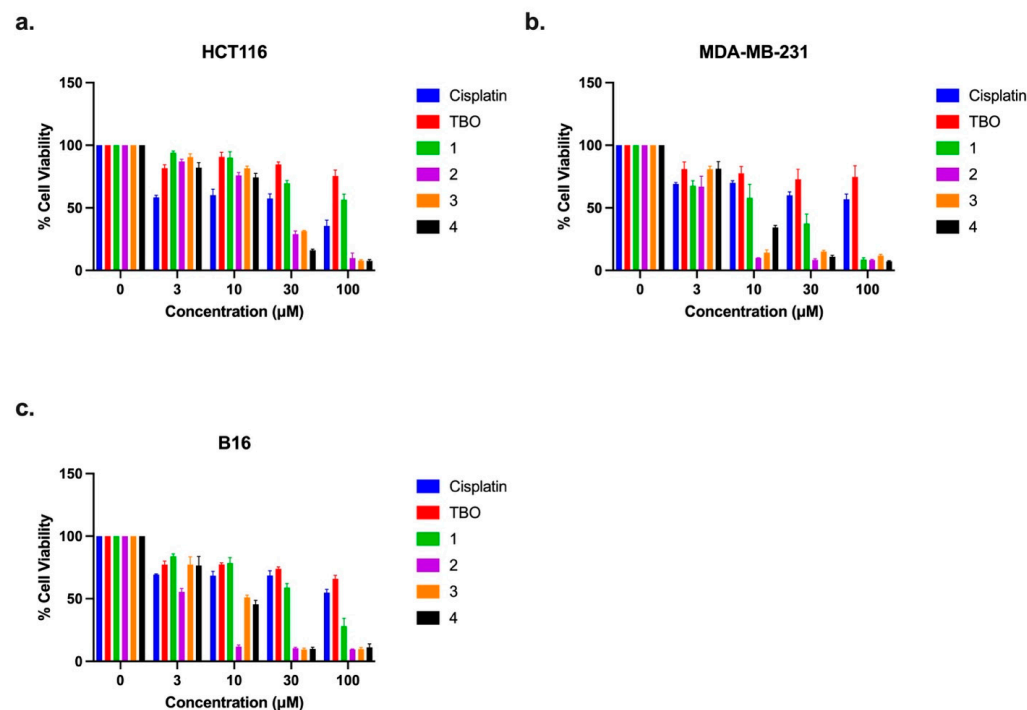
**Table 2.**  $^{13}\text{C}$  NMR chemical shift ( $\delta$ ) of free ligand and its complexes (1–4) carried out in DMSO- $d_6$  solution.

Compounds	C=S	C=N-OH	C=N-N	C1'	C2'	C1	C2	C3	C4
TBO	179.00	154.72	147.46	11.76	9.38	-	-	-	-
1	174.00	154.59	152.77	12.38	9.52	14.71, 14.33	-	-	-
2	174.04	154.50	152.45	12.28	9.42	16.97, 16.61	8.97	-	-
3	174.02	154.50	152.08	12.26	9.41	29.55	31.80	-	-
4	176.59	154.60	149.73	12.00	9.38		133.99–129.66		

### 3.3. Evaluation of Novel Complexes (1–4)

The cell viability assessment of novel complexes (TBO, 1, 2, 3, and 4) was accomplished by MTT assay. Three cell lines: HCT-116, MDA-231, and B16 were exposed to the five novel complexes, in addition to cisplatin as a positive control, and were monitored for changes in their cellular metabolic activity. The intensification of the MTT signal is interpreted as an increase in metabolic activity and vice versa.

Table 3 represents the relative  $\text{IC}_{50}$  values of the novel complexes (1–4). The lower  $\text{IC}_{50}$  values compared to cisplatin establish the potential cytotoxic complexes as effective anticancers, which are the three prospective complexes 2, 3, and 4. All three cell lines (HCT116, MDA-MB-231, and B16) are represented with their percentages of cell viability in Figure 2. HCT116 cells showed enhanced cytotoxic activity of 2, 3, and 4 in higher concentrations (30 and 100  $\mu\text{M}$ ) compared to cisplatin (Figure 2a). In addition, the same complexes 2, 3, and 4 were exhibiting higher cytotoxic activity compared to cisplatin against MDA-MB-231 and B16, which were evident in the 10  $\mu\text{M}$  concentrations and higher (Figure 2b,c). Complex 2 showed a decrease in cell viability starting from 3  $\mu\text{M}$ , with a substantial decline with increased concentrations. This can be an indication of complex 2 as a prospective anticancer agent. Further in vivo studies should be considered for the evaluation of the side-effects profile on major organs and the efficacy properties as anticancer therapy.

**Figure 2.** Effect of the concentration of the novel group and cisplatin on the percentage of viability of the three cell lines; (a) HCT-116 cells, (b) MDA-MB-231, and (c) B16.



**Table 3.** IC<sub>50</sub> values (μM) of normalized cisplatin and the novel complexes on HCT116, MDA-MB-231, and B16 cancer cell lines.

	IC <sub>50</sub> in μM (SD)		
	HCT116	MDA-MB-231	B16
Cisplatin	34.57 ± 1.29	40.05 ± 1.84	69.29 ± 2.1
TBO	>100	>100	>100
1	>100	13.29 ± 4.76	38.72 ± 3.18
2	18.55 ± 2.07	4.83 ± 2.03	2.604 ± 1.01
3	20.59 ± 1.13	5.59 ± 1.29	7.493 ± 2.09
4	14.37 ± 1.84	7.50 ± 1.82	6.592 ± 2.92

### 3.4. Mitochondrial Damage and Induction of Apoptosis by the Novel Complex 2

To study the cytotoxic effects of complex 2 on breast cancer cells by defining apoptosis using JC-1 staining assay,  $\Delta\Psi_m$  disturbance was measured to indicate that MDA-MB-231 cells showed a drop in the aggregate/monomer ratio with increased complex 2 concentrations. The results indicate that MDA-MB-231 cells treated with the novel complex 2 demonstrated a continuous loss of  $\Delta\Psi_m$  with increased concentrations and a significant decrease in the red/green fluorescence intensity ratio in the 3 and 5 μM values ( $p < 0.05$ ) compared with the control (Figure 3). The decline in  $\Delta\Psi_m$  can be interpreted as a dose-dependent loss due to mitochondrial depolarization induced by complex 2. Therefore, the activation of the caspase cascade and the occurrence of apoptosis can be a subsequent event after  $\Delta\Psi_m$  disturbance.

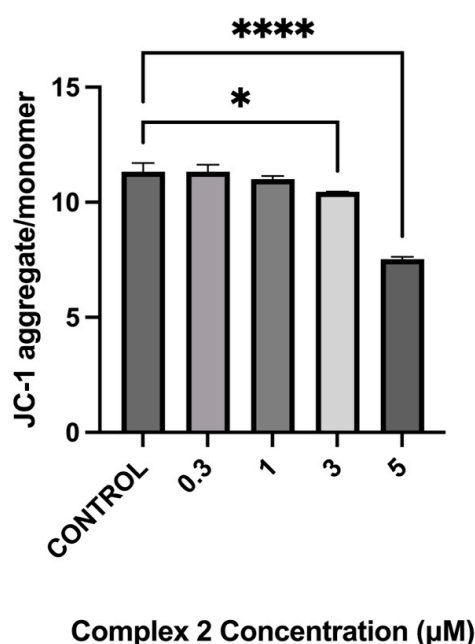


**Figure 3.** The impact of complex 2 on  $\Delta\Psi_m$  in MDA-MB-231 cell line. The  $\Delta\Psi_m$  was measured by JC-1 staining. The data were analyzed by one-way ANOVA, expressed as mean  $\pm$  SD. \*  $p < 0.05$ , and \*\*\*\*  $p < 0.0001$ , compared with control group.

### 3.5. Induction of Mitochondrial ROS and Apoptosis by Complex 2

Elevation in intracellular ROS levels leads to apoptosis by inducing oxidative stress [49]. To accomplish the relationship between the alterations in ROS and complex 2-induced apoptosis, H2DCFDA dye was used. The assay significantly increased fluorescence intensity in the 0.3, 1, and 3 μM concentrations of the novel complex 2 and the positive control H<sub>2</sub>O<sub>2</sub> ( $p < 0.05$ ). The fluorescence intensity indicates higher ROS levels. These observations

support the notion that the novel complex 2 can effectively induce apoptosis by ROS in breast cancer cells. (Figure 4).

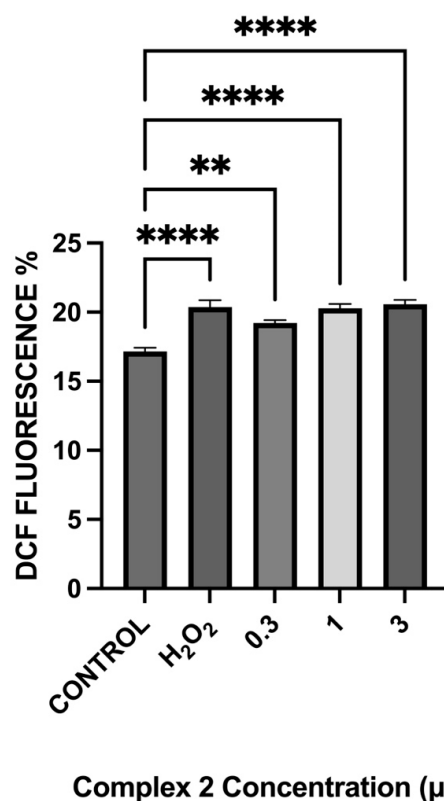


**Figure 4.** The effect of the novel complex 2 on ROS levels in MDA-MB-231 cells. The ROS levels are represented by the percentage increase in the fluorescence intensity of H<sub>2</sub>DCFDA dye. The data were analyzed by one-way ANOVA, expressed as mean  $\pm$  SD. \*\*  $p < 0.01$ , and \*\*\*\*  $p < 0.0001$ , compared with control group.

### 3.6. Complex 2 Induction of Apoptosis by Enhancing the Production of Proapoptotic Gene Expression and Reducing Antiapoptotic Genes in MDA-MB-231 Cells

To understand the molecular mechanism in which the novel complex 2 works, we examined its effects on apoptosis. The quantification of apoptotic genes, with respect to GAPDH as the control, revealed changes in the expression of the proapoptotic gene caspase-3 and antiapoptotic gene BCL-xL. The MDA-MB-231 cells were treated with 0.3, 1, and 3  $\mu$ M concentrations of complex 2 for 24 h; next, the extracted RNA of the treated cells was analyzed. The caspase-3 gene expression levels increased significantly under the complex 2 treatment ( $p < 0.05$ ). As seen in Figure 5a, caspase-3 gene expression levels showed a steady increase, indicating the apoptotic death occurring with increased complex 2 concentrations.

In order to determine the involvement of the antiapoptotic gene BCL-xL, qPCR measurements were taken of BCL-xL in the MDA-MB-231 cell line exposed to different concentrations of complex 2 for 24 h incubation (Figure 5b). There was a slight increase in the level of BCL-xL in the 0.3  $\mu$ M concentration. In addition, both 0.3 and 1  $\mu$ M concentrations did not show significant increase after 24 h complex 2 exposure ( $p > 0.05$ ). Whereas, in the 3  $\mu$ M concentration, complex 2 showed a significantly higher expression compared to the control ( $p < 0.05$ ). The upregulation of the proapoptotic gene caspase-3 as well as the downregulation of the antiapoptotic gene BCL-xL contributes to cell destruction by programmed cell death and mitochondrial dysfunction [50], which was observed after complex 2 treatment.

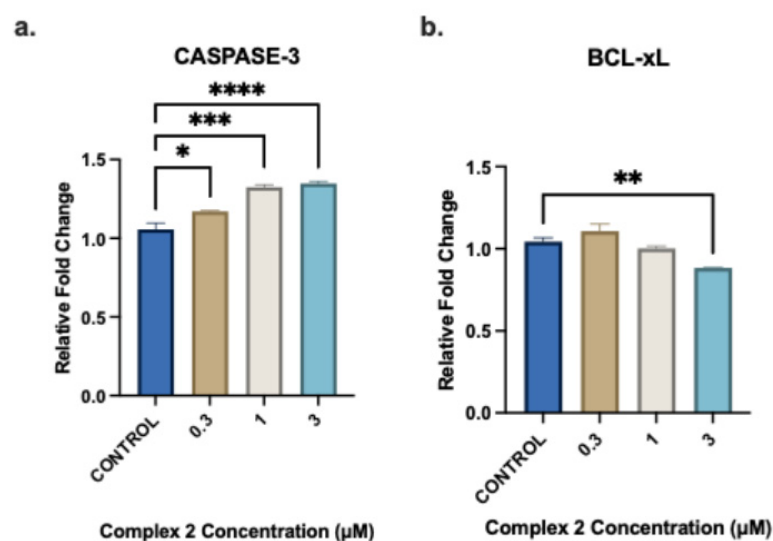


**Figure 5.** The relative fold change of caspase-3 and BCL-xL gene expression in MDA-MB-231 cells treated with complex 2. (a) caspase-3 gene expression levels in MDA-MB-231 cells after complex 2 treatment. (b) BCL-xL gene expression levels in MDA-MB-231 cells after complex 2 treatment. The genes were normalized to GAPDH. The data were analyzed by one-way ANOVA, expressed as mean  $\pm$  SD. \*  $p < 0.05$ , \*\*  $p < 0.01$ , \*\*\*  $p < 0.001$ , and \*\*\*\*  $p < 0.0001$ , compared with control group.

### 3.7. Solution Chemistry of Complexes (1–4)

The stability of complexes 1–4 was assessed by subjecting them to UV-visible spectroscopy at room temperature in DMSO and EtOH:H<sub>2</sub>O (1:1) solutions. The complexes exhibited complete solubility in the respective solutions. Spectral measurements were taken at various time intervals ranging from 0 to 48 h, as illustrated in the Supplementary Figures S20 and S21. Throughout the experiments, no changes were observed in the spectra at different time intervals. There were no noticeable shifts, either red or blue, in the absorption peaks of each complex, nor were there any new absorption peaks observed. These findings strongly indicate that complexes 1–4 remained stable without undergoing decomposition throughout the 48 h duration of the study.

## 4. Discussion

We investigated the novel complexes (TBO, 1, 2, 3, and 4) with cell viability assay in three cell lines: HCT116, MDA-MB-231, and B16 and compared them with cisplatin. The IC<sub>50</sub> values were obtained for each complex. Complexes 2, 3, and 4 exhibited significant effects on each tested cancer cell. The cell proliferation inhibition exhibited by the novel complexes is represented in a dose-dependent manner shown in Figure 2. Similar observations were documented in our previous study that showed the effect of novel gold(III) complexes compared to cisplatin against multiple cell lines (A549, HeLa, MDA-231, and MCF-7), whereas those complexes caused a reduction in cell viability with increased complex concentrations [51].

Due to the novelty of the complexes, their underlying molecular mechanisms are unknown. Therefore, we report here that complex 2 exhibits strong anticancer activity in breast cancer cells via the induction of oxidative stress, mitochondrial dysfunction, and apoptosis. Apoptosis is a form of programmed cell death, which is a process that happens in normal tissue and as a stress response to signals, such as reactive oxygen species [50]. This normal process is utilized in vitro to denote cell viability and identify the efficacy and downstream mechanisms of novel anticancer drugs [51,52].

One of the aspects that lead to apoptosis is oxidative stress and increased superoxide radicals [53]. The excessive production of ROS causes oxidative stress, mediating damage to the DNA and RNA in addition to protein and lipid oxidation [54]. The results of this study show that treatment with the novel complex 2 can induce apoptosis by increased production

of ROS, thus exasperating cytotoxicity. Moreover, to expand on apoptosis ensuing in the cells incubated with this novel complex, mitochondrial membrane potential disruption was usually observed as the early sign of apoptotic death [55]. Consequently, the  $\Delta\Psi_m$  assay using JC-1 dye was performed to observe mitochondrial damage, where the reduction in mitochondrial membrane potential was occurring in a concentration-dependent manner. This disruption in  $\Delta\Psi_m$  is one of the main contributing factors in cellular apoptosis [55].

There are two signaling pathways that can trigger apoptosis: intrinsic and extrinsic pathways [50]. Caspase 3 is a marker of apoptosis, which is termed executioner caspase [56]. The current study examined the molecular mechanism of action of complex 2 on the induction of the apoptotic pathway in vitro, which was investigated by q-RT PCR analyses. Caspase 3 induction was observed after treatment with complex 2, which is indicative that breast cancer cells are undergoing apoptosis, as reported in another study that used venetoclax on the same breast cancer cell line, MDA-MB-231 [57].

In the intrinsic apoptotic pathway, the BCL-2 family proteins are regulators in the molecular mechanisms of apoptosis, which is mediated by mitochondria. They are divided based on their function as proapoptotic and antiapoptotic proteins. Any disruption in the homeostasis between these two groups of proteins can affect the fate of cells [58]. The antiapoptotic BCL-2 family has been overexpressed in several human cancers, leading to resistance to apoptosis and chemotherapy [59]. Previous reports showed that the antiapoptotic BCL-2 proteins maintain mitochondrial membrane integrity and prevent cell death by direct interaction with proapoptotic members [60]. BCL-xL is known to be involved in mitochondrial metabolism and suppression of proapoptotic  $Ca^{2+}$  signaling, indicating its possible involvement in cancer cell death [61].

In the results obtained with MDA-MB-231 cells, there was a downregulation of BCL-xL gene expression. However, in the 0.3  $\mu$ M complex 2 treatments, there was an activation of the BCL-xL. Corresponding to this slight elevation, Al-Khayal et al. denoted that the low concentration of novel anticancer agents elevated the expression of BCL-2 protein [62], which occurs initially in response to chemotherapy. Bessou et al. provided evidence that BCL-xL is essential for cell migration by affecting the production of mitochondrial ROS. The inhibition of BCL-xL decreased overall levels of ROS, thus decreasing cell migration, and later, the overexpression of such protein regained the ROS levels and restored cell migration [63].

The gene expression analyses showed that MDA-MB-231 cells treated with complex 2 increased the proapoptotic gene caspase-3 and decreased the expression of the antiapoptotic gene BCL-xL. Thus, we can conclude that this drug can elicit apoptosis in breast cancer MDA-MB-231 cells, attributing it to the upregulation of caspase-3, downregulation of BCL-xL, and alterations in mitochondrial membrane potential. Complex 2 has a higher anticancer potential than cisplatin and was seen to trigger apoptosis and cytotoxicity by eliciting oxidative stress and mitochondrial damage in breast cancer cell lines.

## 5. Conclusions

This report details the synthesis, characterization, and antitumor properties of novel phosphane-gold(I) complexes containing 3-Thiosemicarbano-butan-2-one oxime (TBO) as the ligand. Spectroscopic data indicated that the TBO ligands coordinate to the Au(I) center via the sulfur atom of thio group. Solution studies of complexes 1–4 demonstrated the high stability of the complexes in DMSO and  $H_2O:EtOH$  (1:1) solvent system. In vitro cytotoxicity assays revealed that complexes 2, 3, and 4 exhibited greater cytotoxicity than cisplatin. Further investigations of complex 2 indicated its potential as an apoptosis-inducing agent in breast cancer MDA-MB-231 cells, with upregulation of caspase-3, downregulation of BCL-xL, and alterations in mitochondrial membrane potential. Taken together, these findings suggest that the newly synthesized complexes hold promise as potent anticancer agents capable of inhibiting cancer cell proliferation. However, further in vitro and in vivo studies are necessary to determine the effect on different cancer cell lines and fully evaluate the efficacy, safety, pharmacokinetics, and potential side effects of the complexes.

**Supplementary Materials:** The following supporting information can be downloaded at <https://www.mdpi.com/article/10.3390/biomedicines11092512/s1>, Tables S1 and S2: CHNS analysis and Mid FT-IR; Table S3: <sup>31</sup>P NMR chemical shifts of phosphane-gold(I) precursors and their complexes with TBO ligand in DMSO. Figures S1–S5: FT-IR spectra data; Figures S6–S19: NMR spectra data; Figures S20 and S21: UV-Vis spectra of the complexes.

**Author Contributions:** Conceptualization, A.A.I.; Methodology, S.A.Z., L.B., H.M.A.S. and M.A.; Validation, H.M.A.S.; Formal analysis, A.A.A.S. and A.A.; Investigation, A.A. and A.A.I.; Writing—original draft, S.A.Z.; Writing—review and editing, A.A.A.S.; Supervision, A.A.A.S.; Project administration, A.A.I. All authors have read and agreed to the published version of the manuscript.

**Funding:** The authors greatly appreciate and are thankful for the financial support provided by King Fahd University of Petroleum and Minerals, Interdisciplinary Research Center for Advanced Materials under project No. INAM2210.

**Institutional Review Board Statement:** Not applicable.

**Informed Consent Statement:** Not applicable.

**Data Availability Statement:** The data are contained within the article or Supplementary Materials.

**Conflicts of Interest:** The authors declare no conflict of interest.

## References

1. Sergeant, N.; Vingtdeux, V.; Eddarkaoui, S.; Gay, M.; Evrard, C.; le Fur, N.; Laurent, C.; Caillierez, R.; Obriot, H.; Larchanché, P.E.; et al. New Piperazine Multi-Effect Drugs Prevent Neurofibrillary Degeneration and Amyloid Deposition, and Preserve Memory in Animal Models of Alzheimer's Disease. *Neurobiol. Dis.* **2019**, *129*, 217–233. [CrossRef] [PubMed]
2. Siegel, R.L.; Miller, K.D.; Jemal, A. Cancer Statistics, 2016. *CA Cancer J. Clin.* **2016**, *66*, 7–30. [CrossRef] [PubMed]
3. Park, G.Y.; Wilson, J.J.; Song, Y.; Lippard, S.J. Phenanthriplatin, a Monofunctional DNA-Binding Platinum Anticancer Drug Candidate with Unusual Potency and Cellular Activity Profile. *Proc. Natl. Acad. Sci. USA* **2012**, *109*, 11987–11992. [CrossRef] [PubMed]
4. Galanski, M.; Jakupec, M.; Keppler, B. Update of the Preclinical Situation of Anticancer Platinum Complexes: Novel Design Strategies and Innovative Analytical Approaches. *Curr. Med. Chem.* **2005**, *12*, 2075–2094. [CrossRef]
5. Cerri, S.; Piccolini, V.M.; Santin, G.; Bottone, M.G.; de Pascali, S.A.; Migoni, D.; Iadarola, P.; Fanizzi, F.P.; Bernocchi, G. The Developmental Neurotoxicity Study of Platinum Compounds. Effects of Cisplatin versus a Novel Pt(II) Complex on Rat Cerebellum. *Neurotoxicol. Teratol.* **2011**, *33*, 273–281. [CrossRef]
6. Galluzzi, L.; Senovilla, L.; Vitale, I.; Michels, J.; Martins, I.; Kepp, O.; Castedo, M.; Kroemer, G. Molecular Mechanisms of Cisplatin Resistance. *Oncogene* **2012**, *31*, 1869–1883. [CrossRef]
7. Argyriou, A.A.; Polychronopoulos, P.; Iconomou, G.; Chroni, E.; Kalofonos, H.P. A Review on Oxaliplatin-Induced Peripheral Nerve Damage. *Cancer Treat. Rev.* **2008**, *34*, 368–377. [CrossRef]
8. Bruijninx, P.C.; Sadler, P.J. New Trends for Metal Complexes with Anticancer Activity. *Curr. Opin. Chem. Biol.* **2008**, *12*, 197–206. [CrossRef]
9. Casas, J.S.; Garcia-Tasende, M.S.; Sordo, J. Main Group Metal Complexes of Semicarbazones and Thiosemicarbazones. A Structural Review. *Coord. Chem. Rev.* **2000**, *209*, 197–261. Available online: [https://www.scrip.org/\(S\(351jmbntvnsjt1aadkposzje\)\)/reference/referencespapers.aspx?referenceid=1749909](https://www.scrip.org/(S(351jmbntvnsjt1aadkposzje))/reference/referencespapers.aspx?referenceid=1749909) (accessed on 4 November 2022). [CrossRef]
10. Lobana, T.S.; Sharma, R.; Bawa, G.; Khanna, S. Bonding and Structure Trends of Thiosemicarbazone Derivatives of Metals—An Overview. *Coord. Chem. Rev.* **2009**, *253*, 977–1055. Available online: <https://www.scrip.org/reference/ReferencesPapers.aspx?ReferenceID=1819711> (accessed on 4 November 2022). [CrossRef]
11. Yildiz, M.; Ünver, H.; Dülger, B.; Erdener, D.; Ocak, N.; Erdönmez, A.; Durlu, T.N. Spectroscopic Study, Antimicrobial Activity and Crystal Structures of N-(2-Hydroxy-5-Nitrobenzalidene)4-Aminomorpholine and N-(2-Hydroxy-1-Naphthylidene)4-Aminomorpholine. *J. Mol. Struct.* **2005**, *738*, 253–260. [CrossRef]
12. Mishra, D.; Naskar, S.; Drew, M.G.B.; Chattopadhyay, S.K. Synthesis, Spectroscopic and Redox Properties of Some Ruthenium(II) Thiosemicarbazone Complexes: Structural Description of Four of These Complexes. *Inorg. Chim. Acta* **2006**, *359*, 585–592. [CrossRef]
13. Basuli, F.; Peng, S.M.; Bhattacharya, S. Unusual Coordination Mode of Thiosemicarbazone Ligands. A Search for the Origin. *Inorg. Chem.* **2000**, *39*, 1120–1127. [CrossRef]
14. Beraldo, H.; Gambino, D. The Wide Pharmacological Versatility of Semicarbazones, Thiosemicarbazones and Their Metal Complexes. *Mini-Rev. Med. Chem.* **2004**, *4*, 31–39. Available online: <https://www.scrip.org/reference/referencespapers.aspx?referenceid=2312425> (accessed on 5 November 2022).
15. West, D.X.; Liberta, A.E.; Padhye, S.B.; Chikate, R.C.; Sonawane, P.B.; Kumbhar, A.S.; Yerande, R.G. Thiosemicarbazone Complexes of Copper(II): Structural and Biological Studies. *Coord. Chem. Rev.* **1993**, *123*, 49–71. [CrossRef]

16. Prabhakaran, R.; Kalaivani, P.; Poornima, P.; Dallemer, F.; Huang, R.; Vijaya Padma, V.; Natarajan, K. Synthesis, DNA/Protein Binding and in Vitro Cytotoxic Studies of New Palladium Metallothiosemicarbazones. *Bioorg. Med. Chem.* **2013**, *21*, 6742–6752. [CrossRef]
17. El-Ayaan, U.; Youssef, M.M.; Al-Shihry, S. Mn(II), Co(II), Zn(II), Fe(III) and U (VI) Complexes of 2-Acetylpyridine 4N-(2-Pyridyl) Thiosemicarbazone (HAPT); Structural, Spectroscopic and Biological Studies. *J. Mol. Struct.* **2009**, *936*, 213–219. [CrossRef]
18. García-Tojal, J.; García-Orad, A.; Díaz, A.A.; Serra, J.L.; Urtiaga, M.K.; Arriortua, M.I.; Rojo, T. Biological activity of complexes derived from pyridine-2-carbaldehyde thiosemicarbazone: Structure of [Co(C7H7N4S)2][NCS]. *J. Inorg. Biochem.* **2001**, *84*, 271–278. [CrossRef]
19. Pelosi, G. Thiosemicarbazone Metal Complexes: From Structure to Activity. *Open Crystallogr. J.* **2010**, *3*, 16–28. [CrossRef]
20. French, F.A.; Blanz, E.J. The Carcinostatic Activity of  $\alpha$ -(N)-Heterocyclic Carboxaldehyde Thiosemicarbazones. I. Isoquinoline-1-Carboxaldehyde Thiosemicarbazone. *Cancer Res.* **1965**, *25*, 1454–1458. Available online: <https://www.scirp.org/reference/ReferencesPapers.aspx?ReferenceID=1823395> (accessed on 5 November 2022).
21. Hosseini-Yazdi, S.A.; Mirzaahmadi, A.; Khandar, A.A.; Eigner, V.; Dušek, M.; Mahdavi, M.; Soltani, S.; Lotfipour, F.; White, J. Reactions of Copper(II), Nickel(II), and Zinc(II) Acetates with a New Water-Soluble 4-Phenylthiosemicarbazone Schiff Base Ligand: Synthesis, Characterization, Unexpected Cyclization, Antimicrobial, Antioxidant, and Anticancer Activities. *Polyhedron* **2017**, *124*, 156–165. [CrossRef]
22. Yuan, J.; Lovejoy, D.B.; Richardson, D.R. Novel Di-2-Pyridyl-Derived Iron Chelators with Marked and Selective Antitumor Activity: In Vitro and in Vivo Assessment. *Blood* **2004**, *104*, 1450–1458. [CrossRef] [PubMed]
23. Cytotoxicity of Copper and Cobalt Complexes of Furfural Semicarbazone and Thiosemicarbazone Derivatives in Murine and Human Tumor Cell Lines—PubMed. Available online: <https://pubmed.ncbi.nlm.nih.gov/11189872/> (accessed on 5 November 2022).
24. Shao, J.; Zhou, B.; di Bilio, A.J.; Zhu, L.; Wang, T.; Qi, C.; Shih, J.; Yen, Y. A Ferrous-Triapine Complex Mediates Formation of Reactive Oxygen Species That Inactivate Human Ribonucleotide Reductase. *Mol. Cancer Ther.* **2006**, *5*, 586–592. [CrossRef] [PubMed]
25. Brockman, R.; Sidwell, R.; Arnett, G.; Shaddix, S. Heterocyclic Thiosemicarbazones Correlation between Structure, Inhibition of Ribonucleotide Reductase, and Inhibition of DNA Viruses. *Exp. Biol. Med.* **1970**, *133*, 609–614. Available online: [https://www.scirp.org/\(S\(351jmbntvnsjt1aadkposzje\)\)/reference/referencespapers.aspx?referenceid=2312426](https://www.scirp.org/(S(351jmbntvnsjt1aadkposzje))/reference/referencespapers.aspx?referenceid=2312426) (accessed on 5 November 2022). [CrossRef]
26. Nomiya, K.; Yamamoto, S.; Noguchi, R.; Yokoyama, H.; Kasuga, N.C.; Ohyama, K.; Kato, C. Ligand-Exchangeability of 2-Coordinate Phosphinegold(I) Complexes with AuSP and AuNP Cores Showing Selective Antimicrobial Activities against Gram-Positive Bacteria. Crystal Structures of [Au(2-Hmpa)(PPh3)] and [Au(6-Hmna)(PPh3)] (2-H2mpa=2-Mercaptopropionic Acid, 6-H2mna=6-Mercaptonicotinic Acid). *J. Inorg. Biochem.* **2003**, *95*, 208–220. [CrossRef]
27. Bostancoğlu, R.B.; İşik, K.; Genç, H.; Benkli, K.; Koparal, A.T. Studies on the Cytotoxic, Apoptotic and Antitumoral Effects of Au(III) and Pt(II) Complexes of 1, 10-Phenanthroline on V79 379A and A549 Cell Lines. *J. Enzym. Inhib. Med. Chem.* **2012**, *27*, 458–466. [CrossRef]
28. Sulaiman, A.A.A.; Ahmad, S.; Mujahid Hashimi, S.; Alqosaibi, A.I.; Peedikakkal, A.M.P.; Alhoshani, A.; Alsaleh, N.B.; Isab, A.A. Novel Dinuclear Gold(i) Complexes Containing Bis(Diphenylphosphano)Alkanes and (Biphenyl-2-Yl)(Di-Tert-Butyl)Phosphane: Synthesis, Structural Characterization and Anticancer Activity. *New J. Chem.* **2022**, *46*, 16821–16831. [CrossRef]
29. Abogosh, A.K.; Alghanem, M.K.; Ahmad, S.; Al-Asmari, A.; As Sobeai, H.M.; Sulaiman, A.A.A.; Fettouhi, M.; Popoola, S.A.; Alhoshani, A.; Isab, A.A. A Novel Cyclic Dinuclear Gold(i) Complex Induces Anticancer Activity via an Oxidative Stress-Mediated Intrinsic Apoptotic Pathway in MDA-MB-231 Cancer Cells. *Dalton Trans.* **2022**, *51*, 2760–2769. [CrossRef]
30. Adokoh, C.K.; Darkwa, J.; Kinfe, H.H. Synthesis, Characterization and Anticancer Evaluation of Phosphinegold(I) Thiocarbohydrylate Complexes. *Polyhedron* **2017**, *138*, 57–67. [CrossRef]
31. Reddy, T.S.; Privér, S.H.; Mirzadeh, N.; Bhargava, S.K. Anti-Cancer Gold(I) Phosphine Complexes: Cyclic Trimers and Tetramers Containing the P-Au-P Moiety. *J. Inorg. Biochem.* **2017**, *175*, 1–8. [CrossRef]
32. Marzo, T.; Massai, L.; Pratesi, A.; Stefanini, M.; Cirri, D.; Magherini, F.; Becatti, M.; Landini, I.; Nobili, S.; Mini, E.; et al. Replacement of the Thiosugar of Auranofin with Iodide Enhances the Anticancer Potency in a Mouse Model of Ovarian Cancer. *ACS Med. Chem. Lett.* **2019**, *10*, 656–660. [CrossRef] [PubMed]
33. Ang, K.P.; Chan, P.F.; Hamid, R.A. Antiproliferative Activity Exerted by Tricyclohexylphosphane-gold(I) n-Mercaptobenzoate against MCF-7 and A2780 Cell Lines: The Role of P53 Signaling Pathways. *BioMetals* **2020**, *34*, 141–160. [CrossRef] [PubMed]
34. Cui, X.Y.; Park, S.H.; Park, W.H. Auranofin Inhibits the Proliferation of Lung Cancer Cells via Necrosis and Caspase-dependent Apoptosis. *Oncol. Rep.* **2020**, *44*, 2715–2724. [CrossRef] [PubMed]
35. Marzano, C.; Gandin, V.; Folda, A.; Scutari, G.; Bindoli, A.; Rigobello, M.P. Inhibition of Thioredoxin Reductase by Auranofin Induces Apoptosis in Cisplatin-Resistant Human Ovarian Cancer Cells. *Free Radic. Biol. Med.* **2007**, *42*, 872–881. [CrossRef]
36. Onodera, T.; Momose, I.; Kawada, M. Potential Anticancer Activity of Auranofin. *Chem. Pharm. Bull.* **2019**, *67*, 186–191. [CrossRef]
37. Landini, I.; Massai, L.; Cirri, D.; Gamberi, T.; Paoli, P.; Messori, L.; Mini, E.; Nobili, S. Structure-Activity Relationships in a Series of Auranofin Analogues Showing Remarkable Antiproliferative Properties. *J. Inorg. Biochem.* **2020**, *208*, 111079. [CrossRef]

38. Tavares, T.T.; Azevedo, G.C.; Garcia, A.; Carpanez, A.G.; Lewer, P.M.; Paschoal, D.; Müller, B.L.; dos Santos, H.F.; Matos, R.C.; Silva, H.; et al. Gold(I) Complexes with Aryl-Thiosemicarbazones: Molecular Modeling, Synthesis, Cytotoxicity and TrxR Inhibition. *Polyhedron* **2017**, *132*, 95–104. [[CrossRef](#)]
39. González-Barcia, L.M.; Fernández-Fariña, S.; Rodríguez-Silva, L.; Bermejo, M.R.; González-Noya, A.M.; Pedrido, R. Comparative Study of the Antitumoral Activity of Phosphine-Thiosemicarbazone Gold(I) Complexes Obtained by Different Methodologies. *J. Inorg. Biochem.* **2020**, *203*, 110931. [[CrossRef](#)]
40. El-Tabl, A.S.; El-Wahed, M.M.A.; Rezk, A.M.S.M. Cytotoxic Behavior and Spectroscopic Characterization of Metal Complexes of Ethylacetoacetate Bis(Thiosemicarbazone) Ligand. *Spectrochim. Acta A Mol. Biomol. Spectrosc.* **2014**, *117*, 772–788. [[CrossRef](#)]
41. Ateş, D.; Gulcan, M.; Gümüş, S.; Şekerci, M.; Özdemir, S.; Şahin, E.; Çolak, N. Synthesis of Bis(Thiosemicarbazone) Derivatives: Definition, Crystal Structure, Biological Potential and Computational Analysis. *Phosphorus Sulfur Silicon Relat. Elem.* **2018**, *193*, 14–22. [[CrossRef](#)]
42. Jouad, E.M.; Larcher, G.; Allain, A.; Riou, A.; Bouet, G.M.; Khan, M.A.; Thanh, X. Do Synthesis, Structure and Biological Activity of Nickel(II) Complexes of 5-Methyl 2-Furfural Thiosemicarbazone. *J. Inorg. Biochem.* **2001**, *86*, 565–571. [[CrossRef](#)] [[PubMed](#)]
43. El-Tabl, A.S.; El-Saied, F.A.; Plass, W.; Al-Hakimi, A.N. Synthesis, Spectroscopic Characterization and Biological Activity of the Metal Complexes of the Schiff Base Derived from Phenylaminoacetylhydrazide and Dibenzoylmethane. *Spectrochim. Acta A Mol. Biomol. Spectrosc.* **2008**, *71*, 90–99. [[CrossRef](#)] [[PubMed](#)]
44. Rao, C.N.R.; Venkataraghavan, R. The C=S Stretching Frequency and the “-N-C=S Bands” in the Infrared. *Spectrochim. Acta* **1962**, *18*, 541–547. [[CrossRef](#)]
45. Li, S.; Khan, M.H.; Wang, X.; Cai, M.; Zhang, J.; Jiang, M.; Zhang, Z.; Wen, X.A.; Liang, H.; Yang, F. Synthesis of a Series of Novel In(III) 2,6-Diacetylpyridine Bis(Thiosemicarbazide) Complexes: Structure, Anticancer Function and Mechanism. *Dalton Trans.* **2020**, *49*, 17207–17220. [[CrossRef](#)] [[PubMed](#)]
46. Jeragh, B.; El-Asmy, A.A. Coordination of Fe(III), Co(II), Ni(II), Cu(II), Zn(II), Cd(II), Hg(II), Pd(II) and Pt(II) with 2,5-Hexanedione Bis(Thiosemicarbazone), HBTS: Crystal Structure of Cis-[Pd(HBTS)]Cl<sub>2</sub> and 1-(2,5-Dimethyl-1H-Pyrrol-1-yl)-Thiourea. *Spectrochim. Acta A Mol. Biomol. Spectrosc.* **2014**, *130*, 546–552. [[CrossRef](#)] [[PubMed](#)]
47. Pedrido, R.; González-Noya, A.M.; Romero, M.J.; Martínez-Calvo, M.; Vázquez López, M.; Gómez-Fórneas, E.; Zaragoza, G.; Bermejo, M.R. Pentadentate Thiosemicarbazones as Versatile Chelating Systems. A Comparative Structural Study of Their Metallic Complexes. *Dalton Trans.* **2008**, *47*, 6776–6787. [[CrossRef](#)] [[PubMed](#)]
48. Hosseini-Yazdi, S.A.; Mirzaahmadi, A.; Khandar, A.A.; Eigner, V.; Dušek, M.; Lotfipour, F.; Mahdavi, M.; Soltani, S.; Dehghan, G. Synthesis, Characterization and in Vitro Biological Activities of New Water-Soluble Copper(II), Zinc(II), and Nickel(II) Complexes with Sulfonato-Substituted Schiff Base Ligand. *Inorg. Chim. Acta* **2017**, *458*, 171–180. [[CrossRef](#)]
49. Dickerson, T.; Jauregui, C.E.; Teng, Y. Friend or Foe? Mitochondria as a Pharmacological Target in Cancer Treatment. *Future Med. Chem.* **2017**, *9*, 2197–2210. [[CrossRef](#)]
50. Carneiro, B.A.; El-Deiry, W.S.; El-Deiry, W. Targeting Apoptosis in Cancer Therapy. *Nat. Rev. Clin. Oncol.* **2020**, *17*, 395–417. [[CrossRef](#)]
51. Alhoshani, A.; Sulaiman, A.A.A.; Sobeai, H.M.A.; Qamar, W.; Alotaibi, M.; Alhazzani, K.; Monim-Ul-mehboob, M.; Ahmad, S.; Isab, A.A. Anticancer Activity and Apoptosis Induction of Gold(III) Complexes Containing 2,2'-Bipyridine-3,3'-Dicarboxylic Acid and Dithiocarbamates. *Molecules* **2021**, *26*, 3973. [[CrossRef](#)]
52. Zahedifard, M.; Faraj, F.L.; Paydar, M.; Looi, C.Y.; Hajrezaei, M.; Hasanpourghadi, M.; Kamalidehghan, B.; Majid, N.A.; Ali, H.M.; Abdulla, M.A. Synthesis, Characterization and Apoptotic Activity of Quinazolinone Schiff Base Derivatives toward MCF-7 Cells via Intrinsic and Extrinsic Apoptosis Pathways. *Sci. Rep.* **2015**, *5*, 11544. [[CrossRef](#)] [[PubMed](#)]
53. Ray, P.D.; Huang, B.-W.; Tsuji, Y. Reactive Oxygen Species (ROS) Homeostasis and Redox Regulation in Cellular Signaling. *Cell Signal.* **2012**, *24*, 981–990. [[CrossRef](#)] [[PubMed](#)]
54. Azmanova, M.; Pitto-Barry, A. Oxidative Stress in Cancer Therapy: Friend or Enemy? *ChemBioChem* **2022**, *23*, e202100641. [[CrossRef](#)]
55. Jeong, S.-Y.; Seol, D.-W. The Role of Mitochondria in Apoptosis. *J. Biochem. Mol. Biol.* **2008**, *41*, 11–22. [[CrossRef](#)] [[PubMed](#)]
56. Morris, G.; Walker, A.J.; Berk, M.; Maes, M.; Puri, B.K. Cell Death Pathways: A Novel Therapeutic Approach for Neuroscientists. *Mol. Neurobiol.* **2018**, *55*, 5767–5786. [[CrossRef](#)] [[PubMed](#)]
57. Alhoshani, A.; Alatawi, F.O.; Fo, A.-A.; Alanazi, F.E.; Attafi, I.M.; Zeidan, A.; Zeidan, A.; Agouni, A.; El Gamal, H.; Shamooun, L.S.; et al. BCL-2 Inhibitor Venetoclax Induces Autophagy-Associated Cell Death, Cell Cycle Arrest, and Apoptosis in Human Breast Cancer Cells. *Oncotargets Ther.* **2020**, *13*, 13357–13370. [[CrossRef](#)]
58. Campbell, K.J.; Tait, S.W.G. Targeting BCL-2 Regulated Apoptosis in Cancer. *Open Biol.* **2018**, *8*, 180002. [[CrossRef](#)]
59. Ramesh, P.; Medema, J.P. BCL-2 Family Deregulation in Colorectal Cancer: Potential for BH3 Mimetics in Therapy. *Apoptosis* **2020**, *25*, 305–320. [[CrossRef](#)]
60. Youle, R.J.; Strasser, A. The BCL-2 Protein Family: Opposing Activities That Mediate Cell Death. *Nat. Rev. Mol. Cell Biol.* **2008**, *9*, 47–59. [[CrossRef](#)]
61. Rosa, N.; Speelman-Rooms, F.; Parys, J.B.; Bultynck, G. Modulation of Ca<sup>2+</sup> Signaling by Antiapoptotic Bcl-2 versus Bcl-XL: From Molecular Mechanisms to Relevance for Cancer Cell Survival. *Biochim. Biophys. Acta Rev. Cancer* **2022**, *1877*, 188791. [[CrossRef](#)]

62. Al-Khayal, K.; Vaali-Mohammed, M.-A.; Elwatidy, M.; Bin Traiki, T.; Al-Obeed, O.; Azam, M.; Khan, Z.; Abdulla, M.; Ahmad, R. Correction to: A Novel Coordination Complex of Platinum (PT) Induces Cell Death in Colorectal Cancer by Altering Redox Balance and Modulating MAPK Pathway. *BMC Cancer* **2020**, *20*, 834. [[CrossRef](#)] [[PubMed](#)]
63. Bessou, M.; Lopez, J.; Gadet, R.; Deygas, M.; Popgeorgiev, N.; Poncet, D.; Nougarede, A.; Billard, P.; Mikaelian, I.; Gonzalo, P.; et al. The Apoptosis Inhibitor Bcl-XL Controls Breast Cancer Cell Migration through Mitochondria-Dependent Reactive Oxygen Species Production. *Oncogene* **2020**, *39*, 3056–3074. [[CrossRef](#)] [[PubMed](#)]

**Disclaimer/Publisher's Note:** The statements, opinions and data contained in all publications are solely those of the individual author(s) and contributor(s) and not of MDPI and/or the editor(s). MDPI and/or the editor(s) disclaim responsibility for any injury to people or property resulting from any ideas, methods, instructions or products referred to in the content.